

HUG: Hierarchical Urban Gaussian Splatting with Block-Based Reconstruction

Zhongtao Wang
Peking University
Beijing, China

Mai Su
Peking University
Beijing, China

Huishan Au
Peking University
Beijing, China

Yilong Li
Peking University
Beijing, China

Xizhe Cao
Peking University
Beijing, China

Chengwei Pan
Beihang University
Beijing, China

Yisong Chen
Peking University
Beijing, China

Guoping Wang
Peking University
Beijing, China

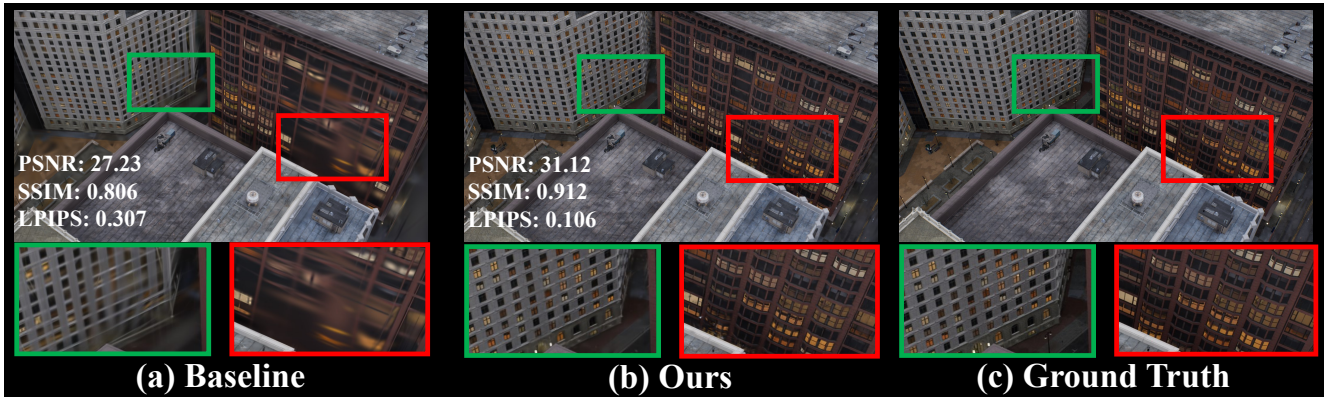


Figure 1. Our method achieves SOTA performance on the *MatrixCity* dataset. In (a), we show the results of the best-performing baseline method. In (b), we present the results of our method, demonstrating clear improvements in visual quality. For reference, (c) displays the Ground Truth. The quantitative metrics (PSNR, SSIM, LPIPS) of this view shown in (a) and (b) highlight the superiority of our approach in terms of reconstruction quality.

Abstract

As urban 3D scenes become increasingly complex and the demand for high-quality rendering grows, efficient scene reconstruction and rendering techniques become crucial. We present **HUG**, a novel approach to address inefficiencies in handling large-scale urban environments and intricate details based on 3D Gaussian splatting. Our method optimizes data partitioning and the reconstruction pipeline by incorporating a hierarchical neural Gaussian representation. We employ an enhanced block-based reconstruction pipeline focusing on improving reconstruction quality within each block and reducing the need for redundant training regions around block boundaries. By integrating neural Gaussian representation with a hierarchical architecture, we achieve high-quality scene rendering at a low computational cost. This is demonstrated by our state-of-

the-art results on public benchmarks, which prove the effectiveness and advantages in large-scale urban scene representation.

1. Introduction

With the increasing complexity of large urban 3D scenes and the growing demand for high-quality rendering, efficient scene reconstruction and rendering techniques have become critical. In recent years, Radiance Field Rendering methods, particularly those based on Neural Radiance Fields [20], have gained significant attention and established themselves as the dominant paradigm for high-quality 3D scene reconstruction and rendering. More recently, 3D Gaussian Splatting [12] has emerged as a promising alternative, offering new possibilities for efficient scene

representation. However, despite their effectiveness, these methods often face inefficiencies when dealing with large-scale scenes or intricate details. To address these challenges, we propose a novel approach named HUG for large-scale urban scene reconstruction and rendering that optimizes both the data partitioning process and the reconstruction pipeline, while incorporating an efficient Level of Detail (LOD) representation.

To reconstruct blocks of large urban scene, many existing methods train large redundant regions around the block boundaries to ensure boundary reconstruction accuracy, resulting in significant computational waste. In contrast, our approach begins with an enhanced block-based reconstruction pipeline that concentrates more on improving reconstruction quality within blocks. By reducing the need for redundant training regions and focusing more on the reconstruction quality within blocks, we release the waste of computing resources, particularly when processing complex or large-scale scenes, and enables improvements in reconstruction quality.

Building upon this foundation, we integrate a neural Gaussian representation with an efficient block-wise hierarchical LOD architecture. This combination ensures high-fidelity scene rendering with low computational cost, regardless of distance. By streamlining computational overhead and maintaining high rendering quality, we enable efficient representation of large-scale scenes without compromising performance.

Finally, we demonstrate the effectiveness of our method by achieving State-of-the-Art (SOTA) results on public benchmarks for large-scale scenes as shown in Figure 1.

Our contributions can be summarized as follows:

- We propose an efficient block-based reconstruction pipeline that optimizes reconstruction quality by cutting unnecessary computational overhead.
- We propose a hierarchical neural Gaussian representation for in-block training and rendering which enables the efficient representation of large-scale scenes.
- We achieve SOTA results on public benchmark datasets, demonstrating the advantages of our approach.

2. Related Work

2.1. Radiance Field Rendering

Radiance field rendering, particularly through Neural Radiance Fields (NeRFs)[2, 3, 19, 20, 24, 25, 32, 34], has made significant strides in 3D scene reconstruction and novel view synthesis. NeRFs represent a scene as a continuous volumetric function, where a deep neural network is trained to map 3D coordinates and viewing directions to radiance and density values. This implicit representation, combined with volumetric rendering, yields highly realistic novel views. However, the method’s dependence on

dense sampling and prolonged network inference times often leads to high computational costs and limits its rendering quality. To address this, several approaches have sought to accelerate NeRF-based rendering. Techniques such as InstantNGP [22] leverage multi-resolution hash grids and compact neural networks to achieve substantial speedups while maintaining high visual fidelity. Mip-NeRF 360 [3] extends NeRF’s capabilities to unbounded scenes while maintaining excellent anti-aliasing and high-quality rendering by properly handling multi-scale observations. Similarly, Plenoxels [9] uses sparse voxel grids to efficiently represent the scene’s continuous density field, delivering notable performance improvements.

Alongside NeRFs, point-based rendering has emerged as an alternative for faster scene rendering. 3D Gaussian Splatting (3DGS)[12] stands out by using 3D Gaussians as primitives, combining explicit geometry with rasterized rendering to enable real-time performance without sacrificing visual quality. Scaffold-GS[18] introduces a hierarchical structure to further improve scene reconstruction. By organizing Gaussians into a scaffold-like framework, this approach enables more accurate and efficient scene representations. Several works have focused on optimizing and compressing Gaussian representations[8, 21], offering inspiration for large-scale, high-quality scene reconstruction. Despite the promise of these works, challenges remain, particularly concerning storage cost when scaling to large scenes.

To tackle the issue of resource saturation, we propose a divide-and-conquer data partitioning strategy that decomposes the environment into manageable regions, ensuring more efficient allocation of computational resources during training. Additionally, we implement a Level-of-Detail system that efficiently adapts the scene’s complexity based on the viewer’s perspective.

2.2. Large Scale Scene Reconstruction

Large-scale scene reconstruction is a challenging problem that involves generating high-fidelity 3D models from extensive data sources. Early approaches[10, 13, 23] restore camera poses using the Structure from Motion (SfM) method. Photo Tourism [28] and Building Rome in a Day [1] rely on large image datasets to generate precise 3D reconstructions. With the emergence of Neural Radiance Fields (NeRF)[20], the paradigm for large-scale scene reconstruction has shifted toward learning-based methods that synthesize photorealistic views of a scene from sparse or incomplete inputs. However, these techniques often face limitations in scaling to large, complex environments due to their high computational and storage demands. To address these issues, recent works such as BlockNeRF[31] and MegaNeRF [33] have employed divide-and-conquer strategies, partitioning scenes into smaller blocks and opti-

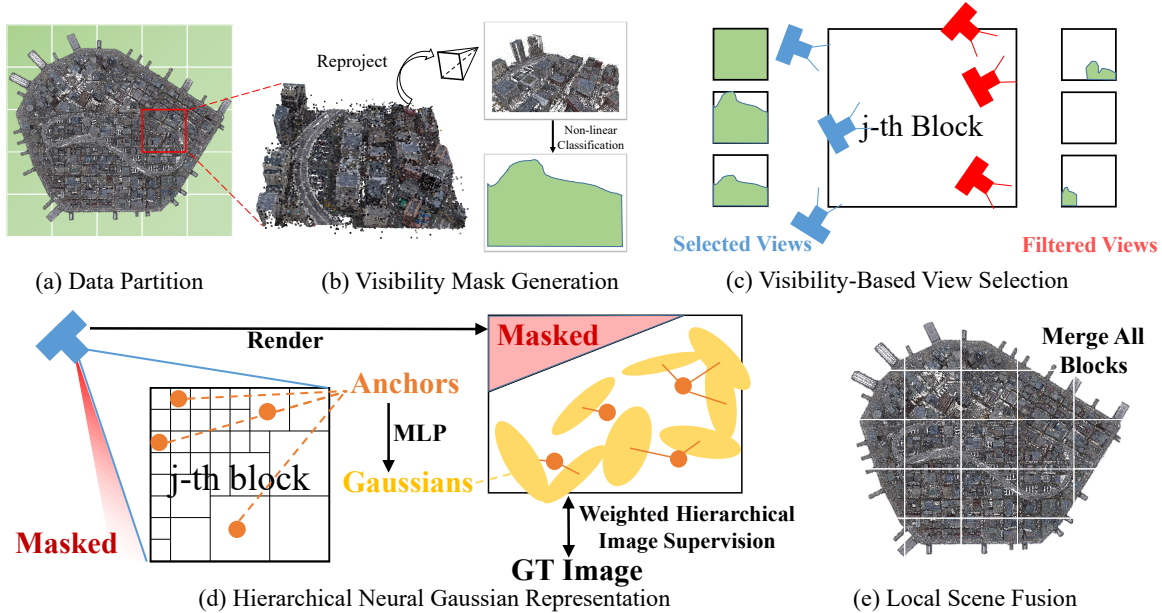


Figure 2. An overview of our proposed method. (a). The sparse point cloud from COLMAP[27] is used to uniformly divide the scene into blocks. (b). For each camera, visibility masks for all blocks are generated by reprojecting 3D points within blocks into the image space and segmenting corresponding visible regions. (c). Cameras are selected for training block j if the visible area in the mask exceeds a threshold. (d). During training each block, anchors within the visibility mask are selected and optimized with our weighted hierarchical supervision, based on their position and level. Then anchors infer the neural Gaussians used for rendering. (e). All the blocks are seamlessly merged and rendered.

mizing each independently, thereby reducing memory consumption. LesGo[7] combined LiDAR point clouds with 3DGS, achieving impressive modeling and rendering quality for large-scale garages. Some recent Gaussian-based approaches[5, 15, 17] also deploy similar strategies to divide large scenes into small blocks and rebuild them respectively. However, these methods train redundant regions around the block boundaries to avoid boundary artifacts, leading to significant computational waste.

Our method addresses these inefficiencies by leveraging the correspondence between geometry and imagery, enabling a targeted reconstruction of the scene’s critical regions. Rather than attempting to reconstruct large surrounding areas, our approach minimizes data redundancy by focusing on the specific regions that require detailed reconstruction. This strategy significantly reduces both computational overhead and memory consumption, offering a more efficient solution for large-scale scene reconstruction.

2.3. Level of Detail Scene Representation

The primary objective of Level-of-Detail (LOD) techniques is to balance computational efficiency with visual fidelity, reducing resource usage for distant or less critical objects while maintaining high-quality rendering. This is achieved by adjusting detail levels based on object proximity or rele-

vance.

In the context of learning scene representations, incorporating LOD has become a significant area of active research. Early efforts like Mip-NeRF [2] and NGLOD [30] have utilized hierarchical representations and multi-resolution voxel grids to represent scenes at varying levels of detail. Unlike NeRF-based methods, the LOD handling in 3DGS scene representation is more intuitive. Several Gaussian-based methods[15, 17] achieve the LOD structure by merging the properties of Gaussian volumes after training all the scenes. We take a different approach by integrating LOD construction directly into the training process. Inspired by Octree-GS[26], we use a framework that combines a hierarchical octree structure with Scaffold-GS [18], our approach enables the simultaneous construction of Level-of-Detail (LOD) details and refinement of the scene representation during training, rather than deferring the generation of a compressed LOD model to later stages.

3. Method

In this section, we introduce HUG, a Hierarchical Urban Gaussian Splatting method designed to efficiently reconstruct and render large-scale urban scenes. An overview of the proposed method is illustrated in Figure 2.

3.1. Preliminary: 3D Gaussian Splatting

3D Gaussian Splatting (3DGS) [12] represents a 3D scene using a set of anisotropic Gaussian primitives. Each Gaussian is defined by a mean position $\boldsymbol{\mu} \in \mathbb{R}^3$ and a covariance matrix $\boldsymbol{\Sigma} \in \mathbb{R}^{3 \times 3}$:

$$G(\boldsymbol{x}) = \exp\left(-\frac{1}{2}(\boldsymbol{x} - \boldsymbol{\mu})^\top \boldsymbol{\Sigma}^{-1}(\boldsymbol{x} - \boldsymbol{\mu})\right), \quad (1)$$

where $\boldsymbol{x} \in \mathbb{R}^3$ is a point in space. Each Gaussian also has an opacity $\alpha \in [0, 1]$ and color features for view-dependent rendering. To synthesize images, Gaussians are projected into the image space using camera parameters, producing 2D Gaussian representations:

$$G'(\boldsymbol{x}') = \exp\left(-\frac{1}{2}(\boldsymbol{x}' - \boldsymbol{\mu}')^\top \boldsymbol{\Sigma}'^{-1}(\boldsymbol{x}' - \boldsymbol{\mu}')\right), \quad (2)$$

where $\boldsymbol{x}' \in \mathbb{R}^2$ is a pixel position. The final image is rendered by compositing these projected Gaussians using alpha blending:

$$C(\boldsymbol{x}') = \sum_i T_i \alpha_i G'_i(\boldsymbol{x}') \boldsymbol{c}_i, \quad T_i = \prod_{j=1}^{i-1} (1 - \alpha_j G'_j(\boldsymbol{x}')), \quad (3)$$

with \boldsymbol{c}_i being the color of the i -th Gaussian. The rendering process is differentiable, allowing optimization of Gaussian parameters by minimizing the difference between rendered and ground truth images.

3.2. Focused Scene Partition Strategy

To facilitate efficient reconstruction of large-scale scenes while conserving computational resources, we propose a focused scene partition strategy. This approach partitions the scene into manageable blocks and selects relevant views for each block based on visibility. By doing so, our method enhances reconstruction quality and minimizes computational redundancy.

Data Partition. Our partitioning approach leverages the sparse point cloud generated by COLMAP [27] as the foundation for dividing the scene. The scene’s bounding box is uniformly divided into multiple blocks indexed by j , ensuring controlled block sizes to prevent memory overflow. Each block will be reconstructed independently, and can be processed in parallel across multiple GPUs and machines, allowing for efficient use of computational resources.

Visibility Mask Generation. For each image I_i and block j , we generate a visibility mask $M_i^j(u, v)$ to indicate which regions of the image correspond to block j . The mask is computed by reprojecting the sparse 3D points of block j into the image space using the camera parameters, followed by non-linear classification to segment the visible

region:

$$M_i^j(u, v) = \begin{cases} 1, & \text{if } (u, v) \text{ corresponds to block } j, \\ 0, & \text{otherwise,} \end{cases} \quad (4)$$

where (u, v) are pixel coordinates in image I_i .

The mask obtained above is used not only in view selection but also in training stage, detailed in Section 3.3. By concentrating on regions that provide crucial information about the target block. We mitigate the computational waste associated with processing Gaussians that may be discarded in later stages, as observed in other works such as CityGS[17] and VastGaussian [15].

Visibility-Based View Selection. To select appropriate views for training block j , we calculate the total visible area of block j in image I_i . An image I_i is included in the training set for block j if the visible area exceeds a threshold τ_p :

$$\sum_{(u,v)} M_i^j(u, v) \geq \tau_p. \quad (5)$$

This ensures that only images that significantly cover block j contribute to its reconstruction, thereby reducing computational waste and enhancing efficiency.

3.3. Hierarchical Neural Gaussian Representation

We employ an Octree-based hierarchical reconstruction strategy to optimize each block. Built upon ScaffoldGS[18] and Octree-GS[26], our system has a combination of LOD and Neural Gaussian capabilities. To the best of our knowledge, we are the first to apply a combination of block-trained neural Gaussians and LOD techniques to the reconstruction and rendering of urban scenes. Although GigaGS[5] also use neural anchors during training, these anchors are discarded after training is completed.

Hierarchical Octree Anchor Initialization Our anchors are initialized at the centers of the nodes of an octree that covers the 3D space. The octree initialization for each block begins with a coarse 3D point cloud P , typically obtained from COLMAP[27] or PixSfM[16]. Following the approach in Octree-GS[26], the maximum level of the octree K is determined by d_{max} and d_{min} , the 0.95 and 0.05 quantiles of distances between all points in P and the camera centers. It is calculated as follows:

$$K = \lfloor \log_2(d_{max}/d_{min}) \rfloor + 1 \quad (6)$$

where $\lfloor \cdot \rfloor$ denotes the rounding operation. Before constructing the octree, we first divide the bounding space of P into 2^{12} subspaces to better represent the scene and prevent the generation of large anchors. For each of the 2^{12} subspaces, starting from the coarsest level 0 to the finest

level $K - 1$, it is subdivided into 8 equal parts at each level to construct the octree, retaining only nodes that contain points from P . The anchors are assigned to the centers of the nodes, with each anchor sharing the same level L as its corresponding node.

Hierarchical Anchor Selection and Optimization For each training view, a predicted level for each visible anchor is calculated as described in Octree-GS[26]:

$$\hat{L} = \lfloor \min(\max(\log_2(d_{max}/d), 0), K - 1) \rfloor \quad (7)$$

where d is the distance between an anchor and this camera center. Only anchors with levels $L \leq \hat{L}$ are then selected for further optimization. As illustrated by the red-marked portion of Figure 3. During optimization, each selected anchor expands into 10 neural Gaussians, each with a explicit offset, neural scaling, rotation, color, and opacity. These neural Gaussians are rendered using same rasterization with 3DGS[12].

In our work, a novel hierarchical training strategy is introduced as shown by the green-marked portion of Figure 3. To enhance hierarchical capabilities and refine details at different levels, each training view will be rendered an additional K times with different LOD levels. We first render anchors with levels $L \leq \hat{L}$ according to Equation 7, the rendered image R_{full} is evaluated with the ground truth image gt using the L1 loss l_1 and SSIM loss l_s losses, weighted by λ and $\gamma = 1 - \lambda$. Then, we render only the anchors with levels equal to $K - 1$, and this rendered image R_{K-1} is measured by the two losses mentioned above, but with weight $\lambda/2^K$ and $\gamma/2^1$, respectively. For anchors with levels equal to $K - 2$, the weights will be $\lambda/2^{K-1}$ and $\gamma/2^2$. This process continues until the level reaches 0. Our hierarchical supervision framework incorporates an opacity mask m_L^o , which addresses the presence of extensive transparent regions that arise when rendering higher-level anchors, as illustrated by level 3 in Figure 3 shows. In addition, a weighting factor θ is introduced to balance the hierarchical component against the full-image content. Accordingly, the hierarchical image-related loss function in our framework can be formulated as follows:

$$\begin{aligned} loss = & \lambda \cdot l_1(gt, R_{full}) + \gamma \cdot l_s(gt, R_{full}) \\ & + \theta \cdot \sum_{k=1}^K \left(\frac{\lambda}{2^{K+1-k}} \cdot l_1(gt, R_{K-k}, m_{K-k}^o) \right. \\ & \left. + \frac{\gamma}{2^k} \cdot l_s(gt, R_{K-k}, m_{K-k}^o) \right) \end{aligned} \quad (8)$$

This approach is designed to render higher-level anchors with greater detail, while lower-level anchors focus on capturing approximate colors to serve as a foundation for fully rendered images, enhancing hierarchical optimization and

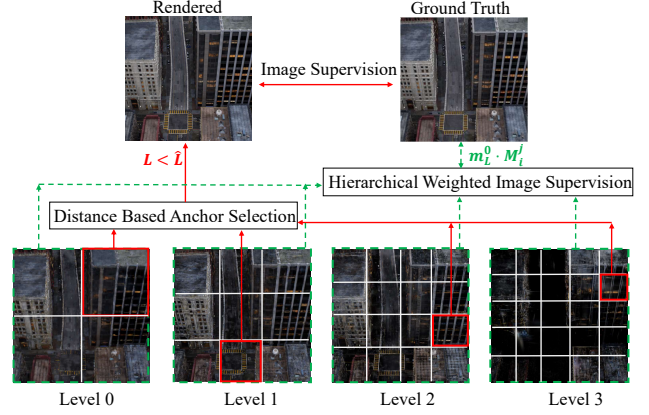


Figure 3. Hierarchical Octree Gaussian Training Strategy. We first select visible anchors based on the distance between the anchor and the camera center across all levels to render a complete scene image. Simultaneously, anchors from different levels are rendered separately, with distinct L1 and SSIM weights applied to evaluate the rendered image at each level.

improving overall image quality. Our hierarchical anchor supervision strategy can greatly resolve an unavoidable issue in OctreeGS[26] that leads to anomalous rendering. More details are shown in supplementary material.

Anchor Splitting and Pruning Splitting the Gaussian or anchors based on the gradient is a common operation and was proposed by 3DGS [12]. In our work, anchors with gradients Δg exceeding a certain threshold τ_g are split into two new anchors with similar properties. For anchors with particularly high gradients, i.e., $\Delta g > \beta \tau_g$ ($\beta > 1$), one generated anchor retains its original level L , while the other is assigned a higher level $L + 1$, as described in Octree-GS [26]. This operation can enhance the refinement of higher-level details. The splitting is discouraged if specific anchor points are located precisely at the target split node. However, our work found that this restriction degrades performance in detail-rich regions. To improve detail rendering in these areas, we removed this limitation. Additionally, as training progresses, an increasing number of anchors tend to average the loss, eventually causing the gradient threshold to become ineffective. Therefore, we also gradually decrease the gradient threshold for splitting during training, $\tau_g(i) = \tau_g \cdot \eta^{i/M}$, where i is the current iteration number, M is the decrease interval, and η is the decrease rate. This greatly improves the splitting efficiency and adaptivity of the training process. To ensure sufficient anchor splitting, we set a percentage threshold τ_s . If the percentage of anchors meeting the splitting criteria falls below τ_s , additional anchors with the highest Δg values within the top τ_s will be manually split.

The Octree-GS[26] also graduallys increase the level of each anchor with a gradient exceeding a threshold smaller than Δ_g , by adding a property L_e . We adopt this strategy in our work as well. However, we found that during training, L_e can exceed 1 or even reach values greater than 2, indicating that the total LOD level K , derived from Equation 6, may lack sufficient detail. Therefore, when the average value of the L_e is larger than 1, we increase the LOD level of the scene by 1, and reset the L_e to lower values. This adjustment allows anchors with higher levels to be generated during the training process.

Pruning anchors or Gaussians based on opacity is a common technique. In addition to this universal pruning strategy, we introduce a visibility-based pruning approach. Since level-related anchor selection is applied in our work, new anchors occasionally appear at incorrect locations with incorrect levels. This results in anchors that retain only their initial properties and are rarely optimized in training views, yet they have to be rendered in test views if they are closer to the test view than to any training views, we show this in the supplementary material. To address this issue, we count the number of times an anchor is selected during training. If this count is below a threshold of ϵ_c , the anchor is pruned. In addition, we track the accumulated gradient of each anchor and prune those with an accumulated gradient smaller than a threshold of ϵ_g .

3.4. Local Scene Fusion and Rendering

Local Scene Refiltering We are the first to introduce neural octree Gaussians to urban scene reconstruction tasks. After training each block in parallel, we refilter the anchors within each block. We apply a non-linear transformation similar to that used in CityGS[17] to map all anchor centers to the range $[-2, 2]$. The bounding box obtained from the block index is then used to refilter the anchors. Since each anchor has 10 neural Gaussians, and the offsets can sometimes be quite large, some anchors may be located inside the bounding box while their neural Gaussians are outside, or vice versa. Therefore, the positions of the neural Gaussians are also considered during the refiltering process. An anchor with more than 5 Gaussians inside the bounding box will be retained in the block, while anchors with fewer than 2 Gaussians inside the bounding box will be discarded, even if the anchor itself is within the block. Refiltered anchors of all blocks are then merged to form a global scene with an additional block index property.

Global Scene Rendering During rendering, we first load the global scene into the GPU. Although each block has a separate MLP network, we load all MLP networks to the GPU and use the block index to select the corresponding MLP network for each anchor. These MLPs are small and require very little GPU memory. The MLP network is used

to calculate the neural properties of the Gaussians, which are then applied to render the scene using differentiable rasterization from 3DGS [12]. This approach enables global scene rendering and viewing without necessitating LOD file loading.

4. Experiments

4.1. Implementation Details

We built our method upon Octree-GS[26] for implementation. We modified the rendering codes and SIBR viewer[4] to support LOD rendering of neural Gaussians generated by MLPs from multiple blocks, enabling real-time rendering of large-scale urban scenes. All source code, datasets, and preprocessing scripts will be made publicly available upon publication.

Our training process consists of two steps. First, we partition the data using the sparse reconstruction results from COLMAP[27], which enables parallel scene reconstruction across multiple GPUs. Specifically, we divide the bounding box into several blocks along the coordinate axes, tailored to the shape of the scene. The sparse points within each block are then projected into image space, and an SVM[6] is used to fit the boundary between inner and outer points after a tenfold downsampling. Additionally, we assign ten times the weight to points within the block, obtaining a mask for the inner and outer parts of the scene in image space. Finally, for each block, we select cameras with a visible area greater than $\tau_p = 10\%$ of the image area to participate in the training of the block’s scene.

In the subsequent phase, we performed block-wise reconstruction initializing from the sparse points seen by selected cameras. These sparse points are preprocessed similar to OctreeGS[26]. We first train for 40,000 iterations as initiation. In this stage, we split or prune anchors every 50 iteration until iteration 30,000, the gradient threshold degeneration factor η is 0.8, and the interval M is 5,000. The Manual splitting ratio τ_s is 0.001. When $mean(L_e) > 1$, we add 1 to the octree level K , and all L_e are divided by 50. For pruning anchors, the visibility count ϵ_c is 5, and accumulated gradient threshold ϵ_g is set as 0.000002. We render anchors of all levels after iteration 10,000. Then our visibility mask and weighted hierarchical supervision are applied for other 40,000 iterations refinement separately. The weight λ between L1 and SSIM is 0.2, the weight θ is set as 0.02. And the opacity mask is $m_L^o > 0.5$. All experiments were conducted on a machine with 8 Nvidia A6000 48GB GPUs and 2 Intel Xeon 6330 CPUs.

4.2. Evaluation

We evaluated our method on four diverse scenes with varying scales and environments. We utilized a synthetic *SMall City* scene from the city-scale dataset, *MatrixCity*[14],

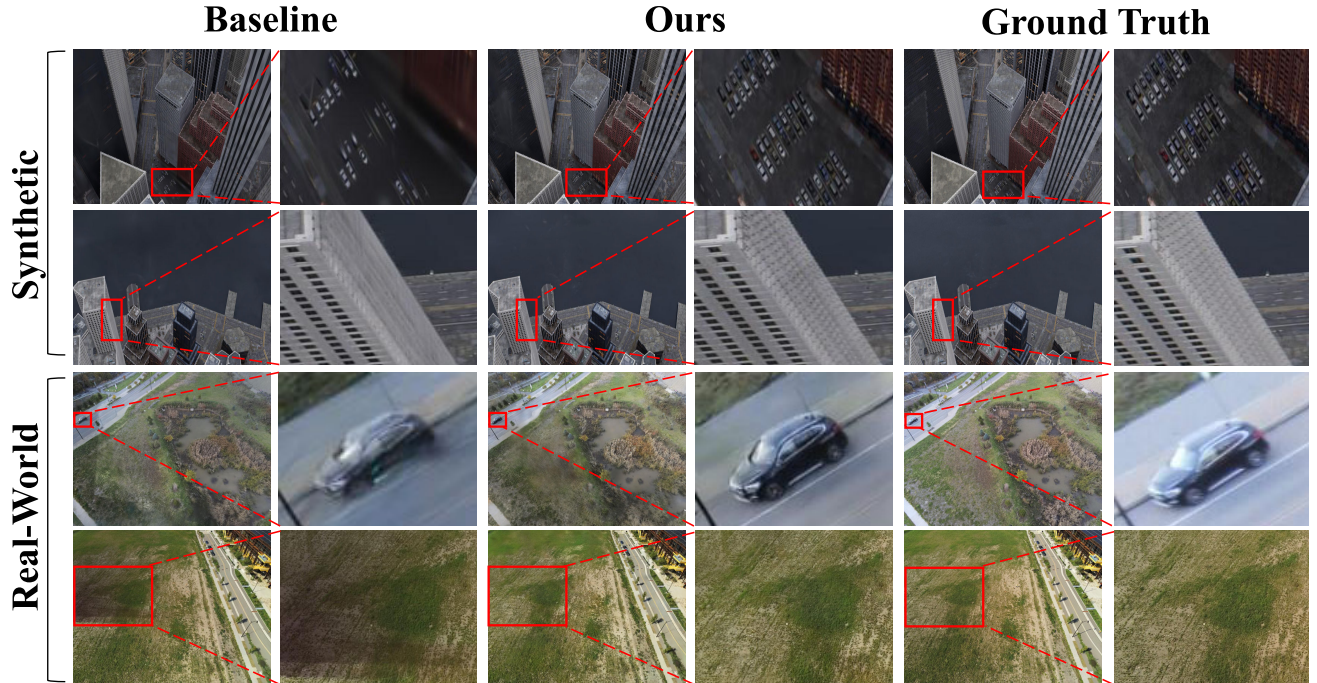


Figure 4. Qualitative comparison with state-of-the-art methods on synthetic and real-world datasets. We select CityGaussian[17] as our sole baseline because it is the only reproducible method evaluated on both synthetic and real-world datasets. Our method reconstructs finer details and produces fewer artifacts compared to baseline.

which is 2.7 km^2 in size. Unlike previous approaches focusing on partial areas[29], we reconstructed the entire city to assess our method’s performance comprehensively. In addition to synthetic data, we conducted experiments on real-world datasets, including *Residence*, *Rubble*, and *Building* from Mega-NeRF[33]. Consistent with prior work[5, 17, 18, 26, 33, 36, 37], we reduced the image resolutions to 1.6k to balance detail and processing time.

For quantitative evaluation, we employed standard metrics: Peak Signal-to-Noise Ratio (**PSNR**), Structural Similarity Index Measure (**SSIM**), and Learned Perceptual Image Patch Similarity (**LPIPS**)[35].

We compared our method against several state-of-the-art baselines, including Mega-NeRF[33], 3DGS[12], CityGaussian[17], and OctreeGS[26].

4.3. Results Analysis

Quantitative Comparisons Table 1 shows the mathematical results, our method achieves SOTA performance compared with novel NeRF-based and Gaussian-based methods on the MatrixCity[14] dataset. Our method outperform OctreeGS[26] over 1.5 PSNR, which shows the effective-

ness of block-based reconstruction and global fusion in our method. We also overwhelm the SOTA method CityGS[29] on this dataset, this proves the effective of our combination of hierarchical representation and neural Gaussian. Our method achieves competitive results on 3 scenes from real world dataset. We again performs better than CityGS, which has similar partition strategy with our work, showing the in-block efficiency of our hierarchical representation and novel fusion technology. We averaged fewer cameras per block than CityGS as shown in the supplement, yet our approach still outperformed theirs.

Qualitative Comparisons Figure 4 showcases qualitative comparisons between our method and the SOTA baseline CityGS[17] on three scenes. Our method produces sharper and more detailed reconstructions, accurately capturing fine textures and structural details with fewer artifacts.

In particular, our reconstructions exhibit better preservation of intricate features such as building facades, textures, and edges. The car we rendered are even clearer than the ground truth. We better restored the lighting intensity of the lawn, showing the effectiveness of our weighted hierarchi-

Table 1. Quantitative comparison of our method with previous approaches. The best scores in each column are highlighted with red background, second best with orange, and third best with yellow. The symbol '-' denotes experiments that are difficult to reproduce.

	MatrixCity			Residence			Rubble			Building		
Metrics	SSIM↑	PSNR↑	LPIPS↓	SSIM↑	PSNR↑	LPIPS↓	SSIM↑	PSNR↑	LPIPS↓	SSIM↑	PSNR↑	LPIPS↓
MegaNeRF[33]	-	-	-	0.628	22.08	0.489	0.553	24.06	0.516	0.547	20.93	0.504
3DGS[12]	0.735	23.67	0.384	0.791	21.44	0.236	0.777	25.47	0.277	0.720	20.46	0.305
Octree-GS[26]	0.814	26.41	0.282	-	-	-	-	-	-	-	-	-
CityGS[17]	0.865	27.46	0.204	0.813	22.00	0.211	0.813	25.77	0.228	0.778	21.55	0.246
Ours	0.883	28.02	0.142	0.804	22.18	0.231	0.796	25.80	0.247	0.761	21.91	0.276

cal supervision. The visual fidelity is consistent across different scenes, highlighting the robustness of our approach.

Efficiency We are the first to introduce a hierarchical neural Gaussian pipeline to urban scene reconstruction task, our main purpose is to allow partitioned parallel training and render the whole urban scene with low memory consumption, we compare with CityGS[17] both in LOD mode and non-LOD mode. The CityGS-LOD mode uses Gaussian compression method LightGaussian[8] to compress Gaussians and reduce computational cost. We render *Rubble* scene with similar visual quality while gradually raising the view center. The results are shown in Figure 5. As the view height increases, both CityGS and CityGS-LOD have a increase in number of Gaussians. But, with our hierarchical representation, the number of Gaussians initially increases and then decreases. Our rendering speed outperforms CityGS, though it is slightly slower than CityGS-LOD. We believe this discrepancy is due to differences in compression rates, and our method involves selecting anchors and predicting neural properties.

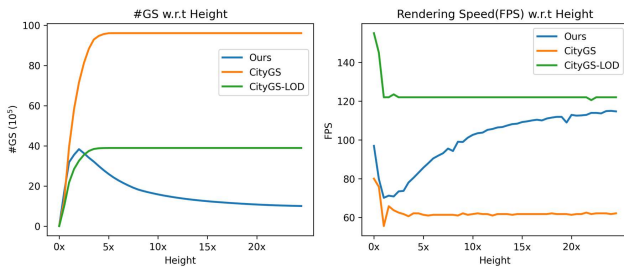


Figure 5. Rendered Gaussian count and FPS performance tested by increasing the camera height in the *Rubble* scene.

4.4. Ablation

To thoroughly evaluate the contributions of each component in our proposed method, we conducted ablation study on the *Building* scene. Specifically, we examined the effects of the usage of the splitting and pruning tricks (S&P) mentioned in Section 3.3, the hierarchical supervision (Hier.) proposed in

Equation 8, and the block-wise focused training (Focused) strategy mentioned in Section 3.2.

Table 2. Ablation on splitting and pruning tricks, hierarchical supervision and focused training.

Model Setting	SSIM ↑	PSNR ↑	LPIPS ↓
w/o S&P	0.695	20.78	0.355
w/o Hier.	0.731	21.12	0.309
w/o Focused	0.749	21.44	0.285
Full model	0.761	21.91	0.276

Splitting and Pruning Strategy Splitting is an important part in Gaussian-based methods, insufficiency of splitting will lead to the degeneration of the rendered image. In our work, we proposed some novel splitting and pruning tricks specifically designed for the hierarchical neural Gaussian urban scene reconstruction task. These tricks can effectively split anchors in detail-rich areas and prune anchors in tricky positions. Our methods is able to increase the LOD levels of the scene automatically. All these functions promise our model higher representation ability and better performance as shown in Table 2.

Hierarchical Supervision In our work, we proposed a novel weighted hierarchical supervision constrain for training layered representations in Equation 8. This supervision compensates for the deficiencies of the anchor selection in OctreeGS[26]. By rendering anchors belonging to different anchors separately, and metric them with different weights, we can effectively learn the hierarchical representations. This supervision effectively guides the model to learn the local and global details of the urban scene, which is crucial for the high quality reconstruction.

Focused Training Strategy Our method employs a block-wise focused training strategy to refine specific regions of the scene by calculating the loss only at locations where the visibility mask equals 1. As shown in Table 2, the block-wise focused training strategy significantly improves reconstruction quality. We believe this is because our strat-

egy reduces the interference from areas with less coverage outside the block on the training within the block.

5. Conclusion

In this paper, we present **HUG**, a novel Hierarchical Urban Gaussian Splatting method designed to efficiently reconstruct and render large-scale urban scenes. The experimental results, demonstrating State-of-the-Art performance on public benchmarks. The efficiency of our HUG for scene reconstruction and rendering sets new standards for urban scene processing.

Despite our approach’s advantages, a few limitations should be addressed in future work. First, our method does not account for dynamic objects or lighting inconsistencies that may exist in real-world large-scale scene datasets. This can be improved by incorporating lighting decoupling and appearance encoding. Second, the data partitioning process relies on the sparse point cloud generated by COLMAP[27], which may lead to issues in low-texture areas that lack sufficient sparse points. Combining pose-free Gaussian methods[11] may help it.

References

- [1] Sameer Agarwal, Yasutaka Furukawa, Noah Snavely, Ian Simon, Brian Curless, Steven M Seitz, and Richard Szeliski. Building rome in a day. *Communications of the ACM*, 54(10):105–112, 2011. 2
- [2] Jonathan T Barron, Ben Mildenhall, Matthew Tancik, Peter Hedman, Ricardo Martin-Brualla, and Pratul P Srinivasan. Mip-nerf: A multiscale representation for anti-aliasing neural radiance fields. In *Proceedings of the IEEE/CVF International Conference on Computer Vision*, pages 5855–5864, 2021. 2, 3
- [3] Jonathan T. Barron, Ben Mildenhall, Dor Verbin, Pratul P. Srinivasan, and Peter Hedman. Mip-nerf 360: Unbounded anti-aliased neural radiance fields. *CVPR*, 2022. 2
- [4] Sebastien Bonopera, Jerome Esnault, Siddhant Prakash, Simon Rodriguez, Theo Thonat, Mehdi Benadel, Gaurav Chaurasia, Julien Philip, and George Drettakis. sibr: A system for image based rendering, 2020. 6
- [5] Junyi Chen, Weicai Ye, Yifan Wang, Danpeng Chen, Di Huang, Wanli Ouyang, Guofeng Zhang, Yu Qiao, and Tong He. Gigags: Scaling up planar-based 3d gaussians for large scene surface reconstruction, 2024. 3, 4, 7
- [6] Corinna Cortes. Support-vector networks. *Machine Learning*, 1995. 6
- [7] Jiadi Cui, Junming Cao, Yuhui Zhong, Liao Wang, Fuqiang Zhao, Penghao Wang, Yifan Chen, Zhipeng He, Lan Xu, Yujiao Shi, et al. Letsgo: Large-scale garage modeling and rendering via lidar-assisted gaussian primitives. *arXiv preprint arXiv:2404.09748*, 2024. 3
- [8] Zhiwen Fan, Kevin Wang, Kairun Wen, Zehao Zhu, De-jia Xu, and Zhangyang Wang. Lightgaussian: Unbounded 3d gaussian compression with 15x reduction and 200+ fps. *arXiv preprint arXiv:2311.17245*, 2023. 2, 8
- [9] Sara Fridovich-Keil, Alex Yu, Matthew Tancik, Qinhong Chen, Benjamin Recht, and Angjoo Kanazawa. Plenoxels: Radiance fields without neural networks. In *Proceedings of the IEEE/CVF Conference on Computer Vision and Pattern Recognition*, pages 5501–5510, 2022. 2
- [10] Christian Fröh and Avidesh Zakhor. An automated method for large-scale, ground-based city model acquisition. *International Journal of Computer Vision*, 60:5–24, 2004. 2
- [11] Sunghwan Hong, Jaewoo Jung, Heeseong Shin, Jisang Han, Jiaolong Yang, Chong Luo, and Seungryong Kim. Pf3plat: Pose-free feed-forward 3d gaussian splatting. *arXiv preprint arXiv:2410.22128*, 2024. 9
- [12] Bernhard Kerbl, Georgios Kopanas, Thomas Leimkühler, and George Drettakis. 3d gaussian splatting for real-time radiance field rendering. *ACM Transactions on Graphics*, 42(4), 2023. 1, 2, 4, 5, 6, 7, 8
- [13] Xiaowei Li, Changchang Wu, Christopher Zach, Svetlana Lazebnik, and Jan-Michael Frahm. Modeling and recognition of landmark image collections using iconic scene graphs. In *Computer Vision—ECCV 2008: 10th European Conference on Computer Vision, Marseille, France, October 12–18, 2008, Proceedings, Part I 10*, pages 427–440. Springer, 2008. 2
- [14] Yixuan Li, Lihan Jiang, Linning Xu, Yuanbo Xiangli, Zhenzhi Wang, Dahua Lin, and Bo Dai. Matrixcity: A large-scale city dataset for city-scale neural rendering and beyond. In *Proceedings of the IEEE/CVF International Conference on Computer Vision*, pages 3205–3215, 2023. 6, 7
- [15] Jiaqi Lin, Zhihao Li, Xiao Tang, Jianzhuang Liu, Shiyong Liu, Jiayue Liu, Yangdi Lu, Xiaofei Wu, Songcen Xu, Youliang Yan, and Wenming Yang. Vastgaussian: Vast 3d gaussians for large scene reconstruction. In *CVPR*, 2024. 3, 4
- [16] Philipp Lindenberger, Paul-Edouard Sarlin, Viktor Larsson, and Marc Pollefeys. Pixel-Perfect Structure-from-Motion with Featuremetric Refinement. In *ICCV*, 2021. 4
- [17] Yang Liu, He Guan, Chuanchen Luo, Lue Fan, Naiyan Wang, Junran Peng, and Zhaoxiang Zhang. Citygaussian: Real-time high-quality large-scale scene rendering with gaussians. 2024. 3, 4, 6, 7, 8, 1
- [18] Tao Lu, Mulin Yu, Linning Xu, Yuanbo Xiangli, Limin Wang, Dahua Lin, and Bo Dai. Scaffold-gs: Structured 3d gaussians for view-adaptive rendering. *arXiv preprint arXiv:2312.00109*, 2023. 2, 3, 4, 7
- [19] Ricardo Martin-Brualla, Noha Radwan, Mehdi SM Sajjadi, Jonathan T Barron, Alexey Dosovitskiy, and Daniel Duckworth. Nerf in the wild: Neural radiance fields for unconstrained photo collections. In *Proceedings of the IEEE/CVF Conference on Computer Vision and Pattern Recognition*, pages 7210–7219, 2021. 2
- [20] Ben Mildenhall, Pratul P Srinivasan, Matthew Tancik, Jonathan T Barron, Ravi Ramamoorthi, and Ren Ng. Nerf: Representing scenes as neural radiance fields for view synthesis. *Communications of the ACM*, 65(1):99–106, 2021. 1, 2
- [21] Wieland Morgenstern, Florian Barthel, Anna Hilsmann, and Peter Eisert. Compact 3d scene representation via self-organizing gaussian grids. *arXiv preprint arXiv:2312.13299*, 2023. 2

- [22] Thomas Müller, Alex Evans, Christoph Schied, and Alexander Keller. Instant neural graphics primitives with a multiresolution hash encoding. *ACM Transactions on Graphics (TOG)*, 41(4):1–15, 2022. [2](#)
- [23] Marc Pollefeys, David Nistér, J-M Frahm, Amir Akbarzadeh, Philippos Mordohai, Brian Clipp, Chris Engels, David Gallup, S-J Kim, Paul Merrell, et al. Detailed real-time urban 3d reconstruction from video. *International Journal of Computer Vision*, 78:143–167, 2008. [2](#)
- [24] Albert Pumarola, Enric Corona, Gerard Pons-Moll, and Francesc Moreno-Noguer. D-nerf: Neural radiance fields for dynamic scenes. In *Proceedings of the IEEE/CVF Conference on Computer Vision and Pattern Recognition*, pages 10318–10327, 2021. [2](#)
- [25] Christian Reiser, Rick Szeliski, Dor Verbin, Pratul Srinivasan, Ben Mildenhall, Andreas Geiger, Jon Barron, and Peter Hedman. Merf: Memory-efficient radiance fields for real-time view synthesis in unbounded scenes. *ACM Transactions on Graphics (TOG)*, 42(4):1–12, 2023. [2](#)
- [26] Kerui Ren, Lihan Jiang, Tao Lu, Mulin Yu, Linning Xu, Zhangkai Ni, and Bo Dai. Octree-gs: Towards consistent real-time rendering with lod-structured 3d gaussians, 2024. [3](#), [4](#), [5](#), [6](#), [7](#), [8](#)
- [27] Johannes Lutz Schönberger and Jan-Michael Frahm. Structure-from-motion revisited. In *Conference on Computer Vision and Pattern Recognition (CVPR)*, 2016. [3](#), [4](#), [6](#), [9](#)
- [28] Noah Snavely, Steven M Seitz, and Richard Szeliski. Photo tourism: exploring photo collections in 3d. In *ACM siggraph 2006 papers*, pages 835–846. 2006. [2](#)
- [29] Kaiwen Song and Juyong Zhang. City-on-web: Real-time neural rendering of large-scale scenes on the web. *arXiv preprint arXiv:2312.16457*, 2023. [7](#)
- [30] Towaki Takikawa, Joey Litalien, Kangxue Yin, Karsten Kreis, Charles Loop, Derek Nowrouzezahrai, Alec Jacobson, Morgan McGuire, and Sanja Fidler. Neural geometric level of detail: Real-time rendering with implicit 3d shapes. In *Proceedings of the IEEE/CVF Conference on Computer Vision and Pattern Recognition*, pages 11358–11367, 2021. [3](#)
- [31] Matthew Tancik, Vincent Casser, Xinchun Yan, Sabeek Pradhan, Ben Mildenhall, Pratul P Srinivasan, Jonathan T Barron, and Henrik Kretzschmar. Block-nerf: Scalable large scene neural view synthesis. In *Proceedings of the IEEE/CVF Conference on Computer Vision and Pattern Recognition*, pages 8248–8258, 2022. [2](#)
- [32] Matthew Tancik, Ethan Weber, Evonne Ng, Ruilong Li, Brent Yi, Terrance Wang, Alexander Kristoffersen, Jake Austin, Kamyar Salahi, Abhik Ahuja, et al. Nerfstudio: A modular framework for neural radiance field development. In *ACM SIGGRAPH 2023 Conference Proceedings*, pages 1–12, 2023. [2](#)
- [33] Haithem Turki, Deva Ramanan, and Mahadev Satyanarayanan. Mega-nerf: Scalable construction of large-scale nerfs for virtual fly-throughs. In *Proceedings of the IEEE/CVF Conference on Computer Vision and Pattern Recognition*, pages 12922–12931, 2022. [2](#), [7](#), [8](#)
- [34] Dejia Xu, Yifan Jiang, Peihao Wang, Zhiwen Fan, Humphrey Shi, and Zhangyang Wang. Sinnerf: Training neural radiance fields on complex scenes from a single image. In *European Conference on Computer Vision*, pages 736–753. Springer, 2022. [2](#)
- [35] Richard Zhang, Phillip Isola, Alexei A Efros, Eli Shechtman, and Oliver Wang. The unreasonable effectiveness of deep features as a perceptual metric. In *Proceedings of the IEEE conference on computer vision and pattern recognition*, pages 586–595, 2018. [7](#)
- [36] Yuqi Zhang, Guanying Chen, and Shuguang Cui. Efficient large-scale scene representation with a hybrid of high-resolution grid and plane features. *arXiv preprint arXiv:2303.03003*, 2023. [7](#)
- [37] MI Zhenxing and Dan Xu. Switch-nerf: Learning scene decomposition with mixture of experts for large-scale neural radiance fields. In *The Eleventh International Conference on Learning Representations*, 2022. [7](#)

HUG: Hierarchical Urban Gaussian Splatting with Block-Based Reconstruction

Supplementary Material

We provide a more detailed discussion on the necessity of visibility mask, data partitioning results, the demonstration of issues with unoptimized anchor points, and more qualitative comparisons.

6. The Necessity of Visibility Mask

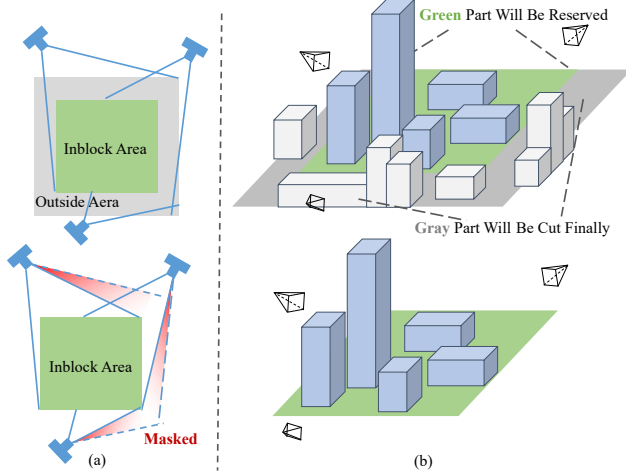


Figure 6. Illustration of the importance of our visibility mask. **(a)**. By employing the visibility mask, our approach efficiently excludes irrelevant regions outside the block, concentrating computational resources on the in-block area. **(b)**. The upper subfigure illustrates the typical approach adopted by most existing methods, where reconstructing a block often entails processing extensive extraneous areas, which are subsequently cut during the fusion step. In contrast, the lower subfigure demonstrates our method, which prioritizes the in-block regions, leading to a more focused reconstruction process.

One of our key observations is that areas outside the reconstruction block do not need to be rebuilt. Existing methods often rebuild extensive regions outside the block, which will be cut during the fusion step. This is depicted as gray areas in Figure 6. By applying the visibility mask, we effectively exclude irrelevant regions from reconstruction, concentrating computational resources on enhancing reconstruction quality within the block. This strategy enables high-quality reconstruction both within the interior of the blocks and at their boundaries without the need to expand the blocks themselves. As a result, we optimize computational efficiency and hardware resource utilization while maintaining control over block sizes and avoiding memory overflow. To achieve this, we apply a non-linear classification method to segment the visible regions from the pro-

jected sparse point cloud.

7. Data Partitioning Results

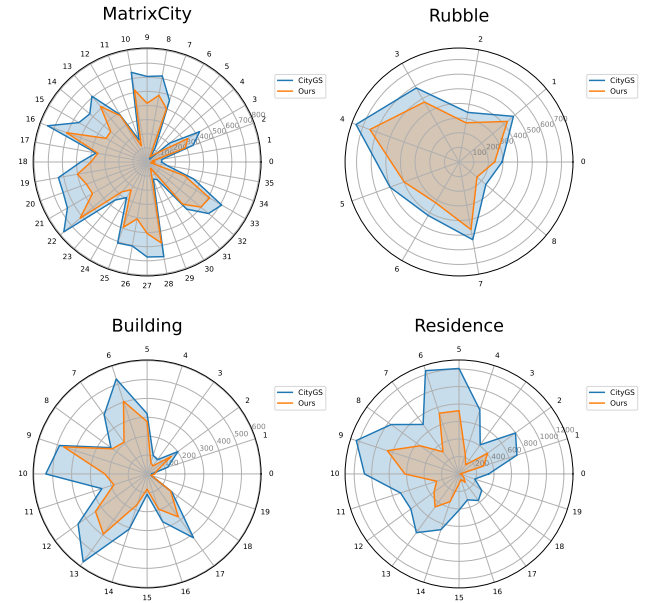


Figure 7. Comparison of the data partitioning results between our method and CityGS[17] across four datasets. The radial coordinate represents the number of training images of each block, while each vertex corresponds to a specific block. It is evident that our method assigns fewer images per block.

To associate all training images with respective blocks, we calculate the total visible area in our generated visibility masks. A threshold of $\tau_p = 10\%$ is then applied to assign each training image to specific blocks. In CityGS[17], a coarse global 3DGS[12] model must first be constructed, after which all images are rendered multiple times corresponding to the number of blocks. As a result, this partitioning process is time-intensive, typically taking hours to complete, e.g., **1.1** hours for the *Rubble* scene. In our method, the partitioning only takes **10** minutes, which is much faster. Moreover, our data partitioning strategy assigns fewer images to each block, reducing memory requirements during training and allowing more resources to be dedicated to reconstructing the in-block area. The number of training images per block is visualized in Figure 7, while the average number is presented in Table 3. We can see that we allocate fewer images to each block, while still achieving better rendering performance as demonstrated in Table 1.

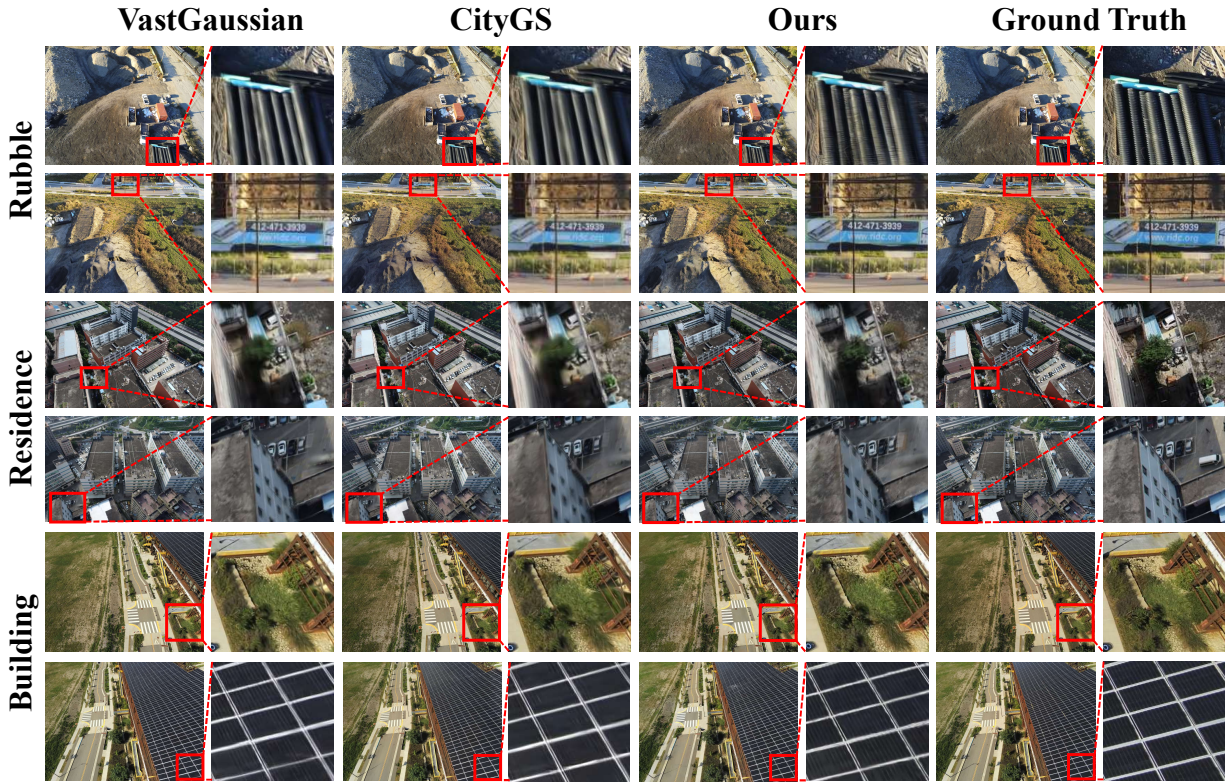


Figure 8. More qualitative comparisons on *Rubble*, *Residence* and *Building* datasets.

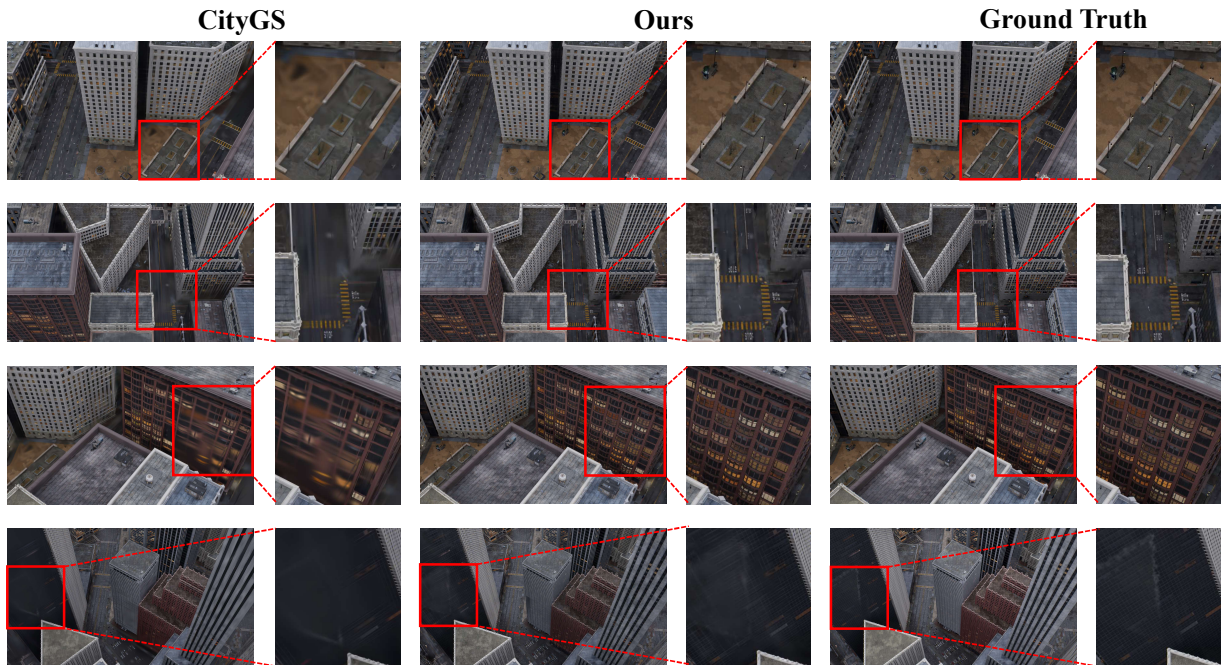


Figure 9. More qualitative comparisons on *MatrixCity* dataset.

Table 3. The average number of training images per block in four scenes.

Methods	MatrixCity	Rubble	Building	Residence
CityGS	438.7	462.0	280.0	697.4
Ours	337.3	379.6	199.8	335.2

8. Demonstration of Issues with Unoptimized Anchor Points

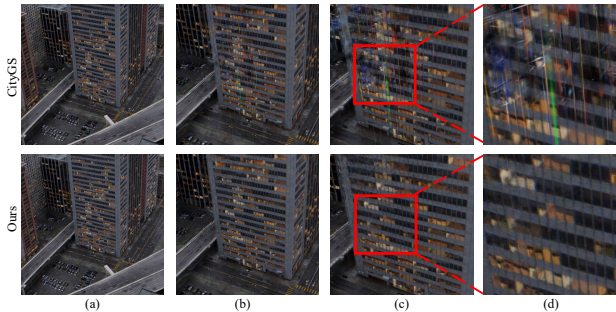


Figure 10. The unoptimized anchor problem. (a). The original rendered view. (b). As the perspective zooms in, some multicolored Gaussians appear. (c). As the perspective zooms in further, more multicolored Gaussians appear, while our method solves this problem. (d). Local zoom-in.

In Octree-GS[26], only anchors with a visibility count greater than a certain threshold are considered for rendering, optimization, and pruning. Additionally, the levels of the anchors are taken into account during training. These strategies enable hierarchical training, but they also introduce some issues. Some anchor points are insufficiently optimized, resulting in reconstruction errors. As shown in the upper row of Figure 10, the anchor points are insufficiently optimized, resulting in the rendering of distorted, multicolored Gaussians. This phenomenon becomes more pronounced as the perspective narrows. In our work, we address this issue through several strategies. First, we prune anchors with a visibility count below a certain threshold $\epsilon_c = 5$. Second, we prune anchors with an accumulated gradient below a specified threshold $\epsilon_g = 0.000002$. Third, we render all visible anchors regardless of their LOD level at certain stages of training. These approaches collectively help optimize the anchor points and reduce reconstruction errors as shown in the lower row in Figure 10.

9. More Qualitative Comparisons

We provide additional qualitative comparisons in Figure 9 and Figure 8. We showcase the rendering results of our method, CityGS[17] and VastGaussian[15]. We do not compare with VastGaussian in our main paper because it has not been open-sourced and is difficult to reproduce. Our

method can render more fine-grained details than CityGS and VastGaussian in Figure 8. We perform better in the textures of pipes, the text on billboards, the details of trees and shrubs, windows, and the patterns of solar panels. In Figure 9, our method outperforms CityGS in areas such as the ground, zebra crossings, streetlights, windows, and the reflection on glass curtain walls.